

## Article

# Preheating Analysis of Semi-Coke in a Circulating Fluidized Bed and Its Kinetic Characteristics

Jiahang Zhang <sup>1,2</sup>, Jianguo Zhu <sup>1,2,\*</sup>  and Jingzhang Liu <sup>1,2</sup>

<sup>1</sup> Institute of Engineering Thermophysics, Chinese Academy of Sciences, Beijing 100190, China; zhangjiahang@iet.cn (J.Z.); liujingzhang@iet.cn (J.L.)

<sup>2</sup> University of Chinese Academy of Sciences, Beijing 100049, China

\* Correspondence: zhujianguo@iet.cn; Tel.: +86-18600052309

**Abstract:** Semi-coke has difficulties with stable ignition and high-efficiency combustion due to its low volatile content. Preheating in a circulating fluidized bed before combustion offers a novel method for the improvement of fuel properties. During preheating, the semi-coke was converted to preheated fuel composed of coal gas and preheated char. When increasing the preheating temperature, the ratio of CO/CO<sub>2</sub> in the coal gas significantly increased, while the ratio of CH<sub>4</sub>/CO<sub>2</sub> remained almost unchanged. After preheating, the release ratios for different species from the semi-coke followed the order C > H > N > S. Thermogravimetric analysis was used to evaluate the kinetic characteristics. We found that the ignition and burnout temperatures of the preheated char decreased compared to those of the semi-coke, and the reaction rate constant for the preheated char increased by 20 times. Three models were used to predict the variations in the conversion ratio with time, and the modified volumetric reaction model showed good agreement with the experiment. This investigation provides support for better developing preheating combustion technology in the future.

**Keywords:** semi-coke; preheating; circulating fluidized bed; kinetic characteristics



**Citation:** Zhang, J.; Zhu, J.; Liu, J. Preheating Analysis of Semi-Coke in a Circulating Fluidized Bed and Its Kinetic Characteristics. *Energies* **2023**, *16*, 4124. <https://doi.org/10.3390/en16104124>

Academic Editors: Yaojie Tu and Qingguo Peng

Received: 8 April 2023

Revised: 11 May 2023

Accepted: 15 May 2023

Published: 16 May 2023



**Copyright:** © 2023 by the authors. Licensee MDPI, Basel, Switzerland. This article is an open access article distributed under the terms and conditions of the Creative Commons Attribution (CC BY) license (<https://creativecommons.org/licenses/by/4.0/>).

## 1. Introduction

Low-rank coal, including lignite and sub-bituminous coal, accounts for more than 50% of reserves, approaching 560 billion tons in China [1]. Pyrolysis is a key step in producing high-value fuel such as coal gas or tar [2,3]. However, several hundred million tons of semi-coke are produced from coal pyrolysis processes every year [4]. Semi-coke has some difficulties with stable ignition and high-efficiency combustion, due to it possessing less than 10% volatile content [5,6].

The co-firing of semi-coke and coal or biomass is a feasible method for combusting low-volatile fuel in a utility boiler. Investigations by Zheng et al. [7] indicated that the semi-coke proportion should be set at <45% to maintain stable combustion. In a 300 MW tangentially fired pulverized coal furnace with a steam pressure of 18.3 MPa and a steam temperature of 535 °C, the maximum ratio of co-firing semi-coke was found to be 40% [8]. When further increasing the ratio of semi-coke supplied to the boiler, unstable combustion, even flameout, can occur, bringing serious challenges for the safe operation of power plants. Wang et al. [9] studied the synergistic effects of coal and semi-coke and found that the interactions between them upon NO formation increased with increasing proportions of semi-coke. However, the co-combustion system was quite complicated, with at least two sets of fuel-feeding equipment, leading to higher investment and operation costs in power plants.

Novel methods or technologies are needed for 100% combustion of semi-coke to overcome the ignition and combustion problems affecting low-volatile fuel. Preheating before combustion, including preheating air or preheating fuel, is undoubtedly a better method to realize stable ignition and high-efficiency combustion [10,11]. Suda et al. [12] preheated air to above 800 °C and achieved high combustion efficiency and low NO<sub>x</sub> emissions for

anthracite. Lv et al. [13,14] preheated semi-coke to above 1000 °C in a first stage and combusted the preheated fuel in a second stage. The results showed that a higher preheating temperature could further lower NO<sub>x</sub> emissions and increase the combustion efficiency. In recent years, another novel preheating method has been proposed by the Institute of Engineering Thermophysics, Chinese Academy of Sciences, with pulverized fuel preheated in a circulating fluidized bed (CFB) [15–17]. However, the conversion characteristics of semi-coke in CFB preheating have not yet been well-elucidated. Importantly, the kinetic characteristics of preheated fuel have not been previously described.

In this work, we conducted an experimental study on semi-coke preheating in a CFB, analyzed the conversion behavior, and built a kinetic model to support the development and application of preheating combustion technology using semi-coke as fuel.

## 2. Experiment

### 2.1. Experimental Apparatus

Figure 1 shows a schematic of the kW-scale preheating combustion experimental platform used in this study, which consisted of a CFB for fuel preheating, a horizontal combustor for preheated fuel combustion, and other auxiliary equipment. The CFB was composed of a riser, a cyclone, and a loop seal.

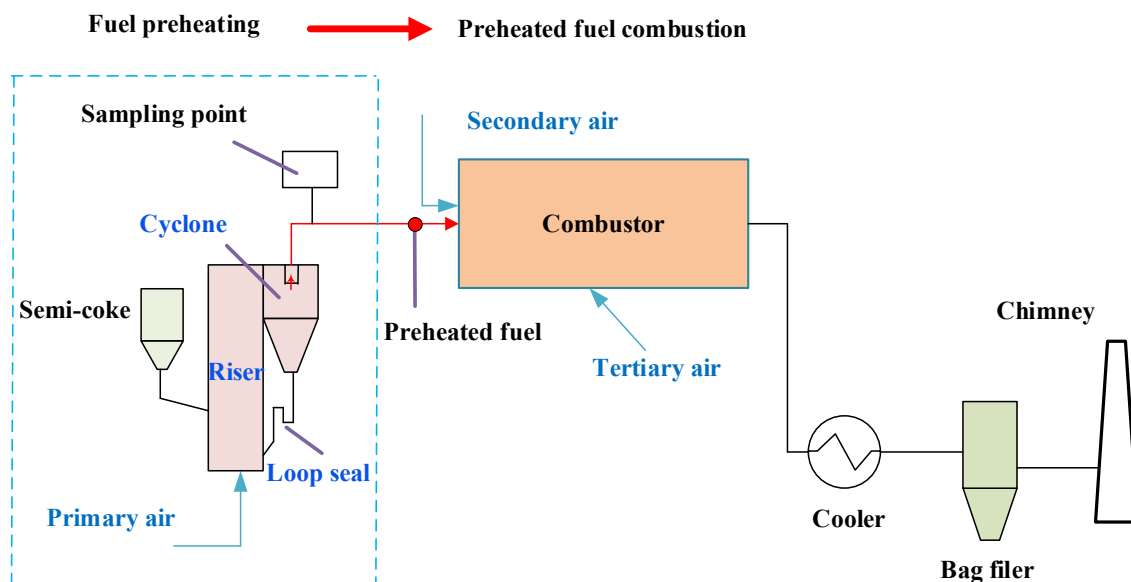


**Figure 1.** The kW-scale preheating combustion experimental platform.

The CFB riser was 81 mm in diameter and 1500 mm in height. In the experiment platform, the primary air flowed into the riser from the air distribution plate positioned at the bottom, and the semi-coke was supplied into the riser via a screw feeder located 250 mm above the air distribution plate. The cyclone was 200 mm in diameter and 400 mm in height, with a center tube of 32 mm diameter inside. The loop seal for transporting material to the riser was 50 mm in diameter. Five K-type thermocouples were used in the CFB, three of which (T1–T3) were 200, 500, and 1450 mm above the air distribution plate, and the other two (T4–T5) were located in the loop seal and the outlet of the cyclone, as shown in Figure 2.

As the amount of primary air was far less than that of the stoichiometric air needed for theoretical combustion, a strong reducing atmosphere was present in the CFB, resulting in some combustion and gasification reactions. In the process of preheating, semi-coke was converted into coal gas and preheated char; i.e., preheated fuel. The relationship between the coal gas flowrate and the preheated char production rate was related to the coal type, preheating temperature, and so on.

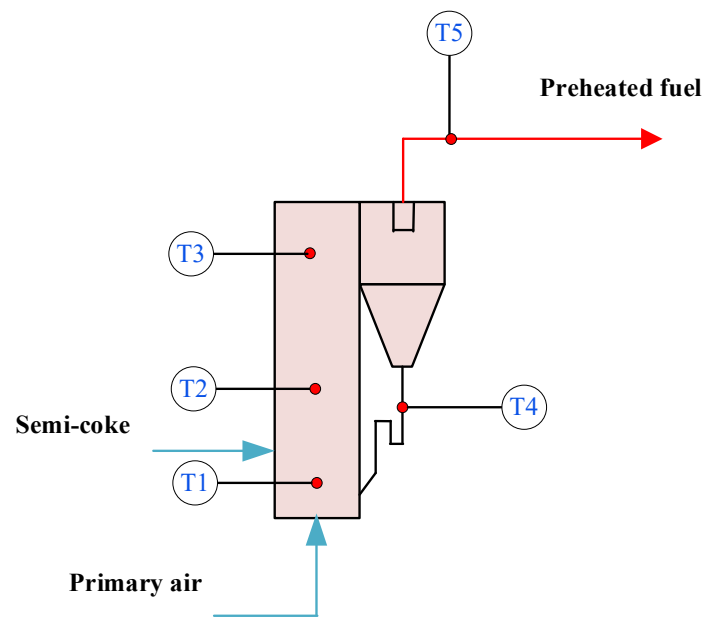


**Figure 2.** The temperature measure points in the CFB.

The horizontal combustor consisted of a square structure with an inner section of  $500 \times 500$  mm and a length of 2115 mm. The preheated fuel flowed into the horizontal combustor through a nozzle with annular secondary air outside. The tertiary air was supplied 1200 mm behind the secondary air inlet.

## 2.2. Fuel Characteristics

The semi-coke used in this experiment was obtained from Shanxi Province, China, and its ultimate and proximate analyses are shown in Table 1. The particle size of the semi-coke ranged from 0 to 0.25 mm, as shown in Figure 3, with a  $d_{50}$  value of  $40 \mu\text{m}$ .

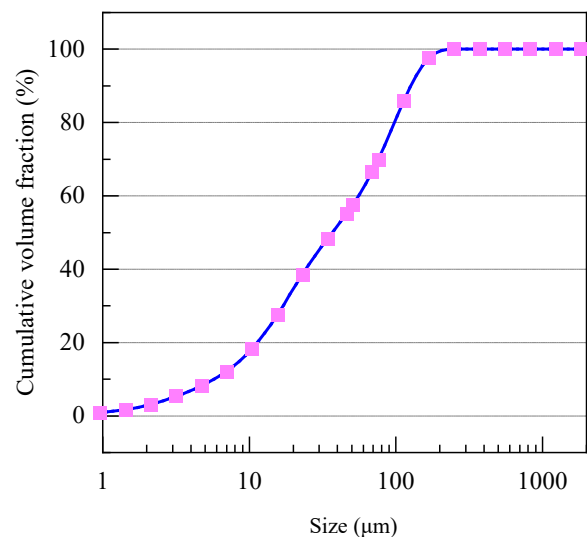


**Figure 3.** Particle size distribution for the semi-coke.

As seen in Table 1, the water content of the semi-coke was 12.80%, which was not very low due to the fact that, during the pyrolysis, the hot semi-coke was directly cooled via water injection; however, this provides beneficial conditions for safe transportation and storage. The volatile matter content was only 4.18%, corresponding to a high fixed carbon content of 76.74%. Compared with bituminous coal, the H and O content in the semi-coke showed an obvious decrease resulting from the pyrolysis itself.

**Table 1.** Proximate and ultimate analyses of the semi-coke.

Item	Proximate Analysis (wt.%)				Ultimate Analysis (wt.%)				
	M <sub>ar</sub>	A <sub>ar</sub>	V <sub>ar</sub>	FC <sub>ar</sub>	C <sub>ar</sub>	H <sub>ar</sub>	O <sub>ar</sub>	N <sub>ar</sub>	S <sub>ar</sub>
Data	12.80	6.28	4.18	76.74	76.81	0.86	2.26	0.67	0.31

Note: the subscript “ar” represents “received basis”.

### 2.3. Experimental Conditions

Table 2 lists the experimental conditions. The preheating temperature was the average temperature at T1, T2, and T3 in the CFB, and  $\lambda_{\text{CFB}}$ ,  $V_{\text{Pr}}$ , and  $\lambda$  indicate the air equivalent ratio in the CFB, the primary air flowrate in the CFB, and the excess air coefficient in the system, respectively. These definitions can be expressed as:

$$\lambda_{\text{CFB}} = V_{\text{Pr}} / V_{\text{Stoic}}, \quad (1)$$

$$\lambda = \frac{V_{\text{Pr}} + V_{\text{Se}} + V_{\text{Te}}}{V_{\text{Stoic}}}, \quad (2)$$

where  $V_{\text{Stoic}}$  is the airflow rate with stoichiometric combustion and  $V_{\text{Pr}}$ ,  $V_{\text{Se}}$ , and  $V_{\text{Te}}$  denote the airflow rates of the primary air, secondary air, and tertiary air, respectively.

$V_{\text{Stoic}}$  can be described by:

$$V_{\text{Stoic}} = F (0.0889(C_{\text{ar}} + 0.375S_{\text{ar}}) + 0.265H_{\text{ar}} - 0.0333O_{\text{ar}}) \quad (3)$$

where  $F$  is the feeding rate for the semi-coke supplied to the CFB and  $C_{\text{ar}}$ ,  $S_{\text{ar}}$ ,  $H_{\text{ar}}$ , and  $O_{\text{ar}}$  represent the ultimate analysis given in Table 1.

**Table 2.** Experimental conditions.

Item	Case One	Case Two	Case Three	Case Four
Feeding rate (kg/h)	3.57	3.56	3.62	3.67
$V_{\text{Stoic}}$ (m <sup>3</sup> /h)	24.9	24.8	25.3	25.6
$\lambda_{\text{CFB}}$	0.3	0.3	0.3	0.3
$V_{\text{Pr}}$ (m <sup>3</sup> /h)	7.5	7.5	7.6	7.7
$V_{\text{Se}}$ (m <sup>3</sup> /h)	12.5	12.5	12.6	12.8
$V_{\text{Te}}$ (m <sup>3</sup> /h)	10.0	10.0	10.1	10.2
$\lambda$	1.20	1.20	1.20	1.20
Preheating temperature (°C)	850	880	910	950

### 2.4. Experimental Procedure and Sample Analysis Methods

At the start of the experiment, 2.5 kg of quartz sand was added to the riser as the bed material, and the primary air was supplied from the air distribution plate. The electric heating device was powered on simultaneously to heat the riser. When the bottom temperature of the riser was approximately 500 °C, bituminous coal for starting up the platform was fed into the riser to raise the bed material temperature. When the average temperature of the riser was approximately 800 °C, the fuel was switched to semi-coke, and the parameters were adjusted to meet the experimental conditions listed in Table 2.

The preheated fuel included coal gas and preheated char, which was collected with a sampling system, as shown in Figure 4, with cooling water to prevent further reactions.

The coal gas composition, including CO, CO<sub>2</sub>, CH<sub>4</sub>, H<sub>2</sub>, O<sub>2</sub>, and C<sub>n</sub>H<sub>m</sub>, was measured online via a Gasboard-3100P gas analyzer. For the preheated char, ultimate, proximate, and thermogravimetric analyses were performed. For the ultimate analysis, the content of carbon, hydrogen, nitrogen, and sulfur was measured with a UNICUBE analyzer (Elementar Company, Langensfeld, Germany), and the oxygen content was

determined with differential calculation. The proximate analysis was carried out according to the Chinese standard GB/T 28731-2012 [18]. The thermogravimetric experiment was performed to analyze the sample mass variations with time using an SAT 449F3 analyzer (NETZSCH Company, Selb, Germany). In the thermogravimetric experiment, the mass of the sample was  $15 \pm 0.2$  mg, and the reaction atmosphere was air at a flow rate of 20 mL/min. The measurement was terminated when the ultimate sample mass remained unchanged.

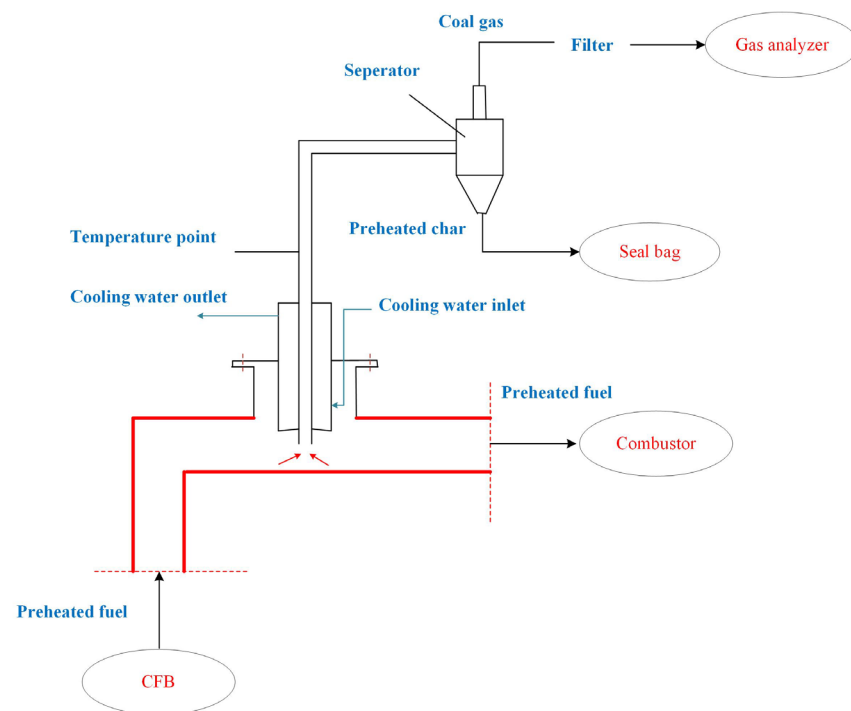


**Figure 4.** The schematic of the preheated fuel sampling.

### 3. Results and Discussion

#### 3.1. Preheating Temperature Variations

The temperature distribution variations with time for case one are shown in Figure 5. The temperatures at each measuring point in the CFB were quite stable, with the temperature differences between the three measurement points (T1, T2, and T3) being below 50 °C. CFBs have the advantage of excellent gas–solid mixing across the entire circuit due to the massive material circulation and have been widely applied in the industry for low-grade fuels, such as coal gangue, coal sludge, and rubbish. At the outlet of the CFB, the preheated fuel temperature was approximately 830 °C, indicating that the semi-coke had completed ignition before flowing into the combustor.

In conventional combustion, the process of ignition and combustion of fuel occurs in the boiler or combustor. If there is a low boiler load, it is extremely difficult to maintain a stable flame and ensure safe operation. Compared with conventional pulverized coal-firing technology, the big difference is that the preheated fuel with a temperature higher than 800 °C flows into the combustor, forming a stable flame and leading to the ignition and combustion in separated equipment. Preheating in a CFB before combustion could offer an advanced, feasible, and economical solution to overcome the combustion problems caused by low-volatile fuel.

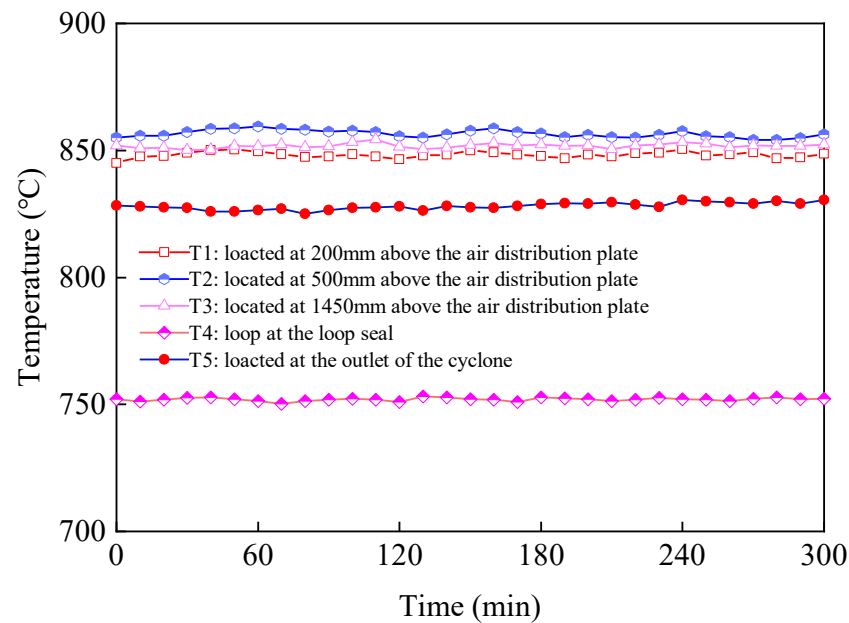


Figure 5. Temperature variations in the CFB with time.

### 3.2. Coal Gas Components

The main coal gas components in cases one to four for the four preheating temperatures are depicted in Figure 6 with the same primary air equivalence ratio of 0.3.

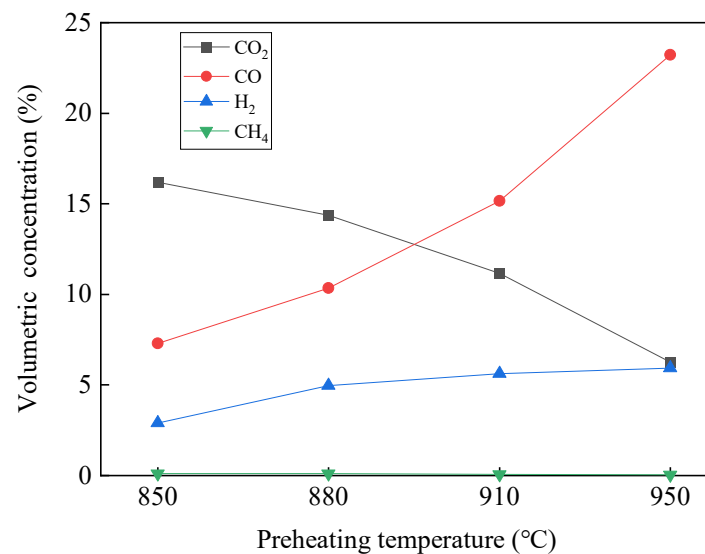


Figure 6. Coal gas components with different preheating temperatures.

As shown in Figure 6, when the CO and H<sub>2</sub> content increased, the CO<sub>2</sub> content decreased, and the CH<sub>4</sub> content remained unchanged as the preheating temperature increased.

The CO increased due to the following two reactions [19]:

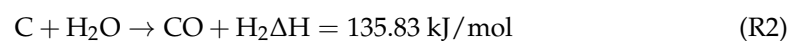
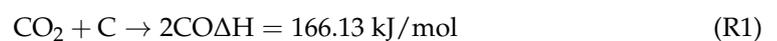


Figure 6 also shows that, at temperatures higher than 900 °C and a primary air equivalence ratio of 0.3, the (R1) reaction resulting in semi-coke gasification was enhanced in the CFB. When the primary air equivalence ratio remained unchanged, the CO concentration

still increased with a further increase in the preheating temperature. The CH<sub>4</sub> concentration was about zero with the different preheating temperatures, as seen in Figure 6, which was due to the fuel itself. As known from previous research, the semi-coke was a by-product of the coal pyrolysis, and the CH<sub>4</sub> in the coal was extracted during the pyrolysis. Furthermore, the synthesis reaction of CO<sub>2</sub> with H<sub>2</sub> resulting in CH<sub>4</sub> is impossible without catalysts.

In accordance with the content of the coal gas components, the heating value for the coal gas could be calculated. The coal gas production rate was determined using the N<sub>2</sub> balance method based on the hypothesis that the nitrogen flowrate would remain unchanged before and after preheating. The formula is expressed as follows:

$$Y_{\text{Gas}} = \frac{0.79V_{\text{Pr}}}{X_{\text{N}_2} \times F_{\text{In}}}, \quad (4)$$

where  $Y_{\text{Gas}}$  is the production rate for coal gas (m<sup>3</sup>/kg),  $X_{\text{N}_2}$  is the content of nitrogen in the coal gas, and  $F_{\text{In}}$  is the feeding rate for semi-coke supplied into the CFB (kg/h).

As a result, the coal gas production rates and heating values with different preheating temperatures were calculated and are shown in Figure 7.

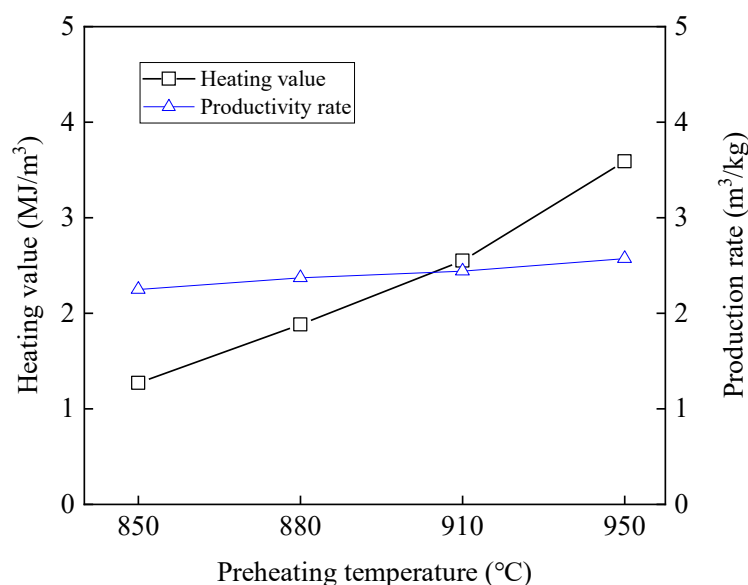


**Figure 7.** The heating values and production rates for the coal gas with different preheating temperatures.

When the preheating temperature increased from 850 °C to 950 °C, the heating value and production rate for the coal gas increased. The increase in the heating value for the coal gas was larger, while the increase in the production rate for the coal gas was quite small. The maximum heating and production rate values for the coal gas were 3.7 MJ/m<sup>3</sup> and 2.57 m<sup>3</sup>/kg, respectively.

To further analyze the intensities of the gasification and combustion reactions, the ratios of CO/CO<sub>2</sub> and CH<sub>4</sub>/CO<sub>2</sub> with different preheating temperatures were calculated, as shown in Figure 8.

As shown in Figure 8, with increasing preheating temperature, the CO/CO<sub>2</sub> ratio increased while the CH<sub>4</sub>/CO<sub>2</sub> ratio remained unchanged due to the dominance of the gasification reaction. Notably, if the air equivalence ratio had varied, the tendency of the CO/CO<sub>2</sub> would have been different.

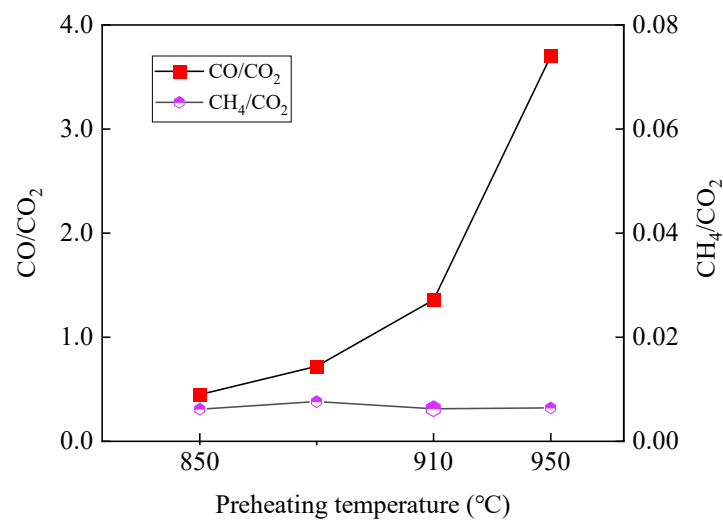


**Figure 8.** The ratios of CO/CO<sub>2</sub> and CH<sub>4</sub>/CO<sub>2</sub> with different preheating temperatures.

### 3.3. Preheated Char Characteristics

The preheated char was collected at the outlet of the CFB, and the particle sizes for the preheated char, semi-coke, and quartz sand supplied to the CFB as bed material are shown in Figure 9.

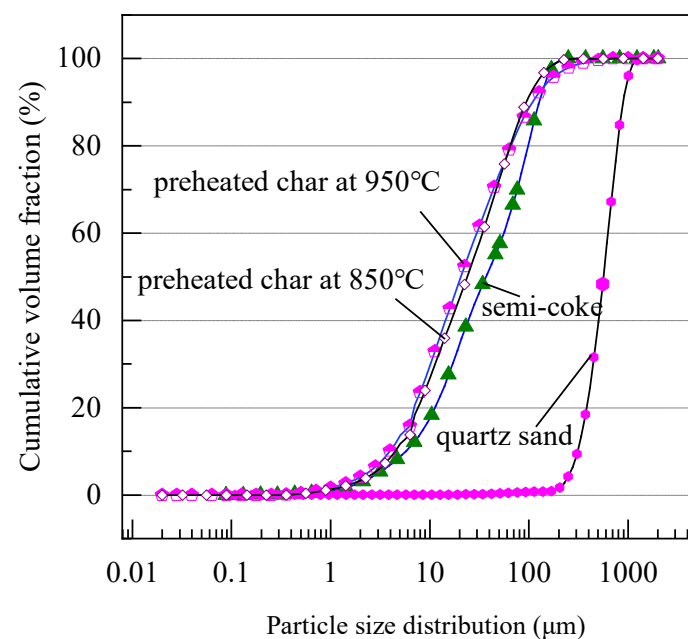


**Figure 9.** Particle size distributions for preheated char, semi-coke, and quartz sand.

Due to the smallest particle size being larger than 0.1 mm, the quartz sand was fully separated out by the cyclone to the loop seal, meaning that the preheated fuel flowing into the combustor was not mixed with quartz sand. Compared with the semi-coke, the particles of the preheated char became finer after preheating because of the breakthrough of particles in the CFB.

The proximate and ultimate analyses of the preheated char are listed in Table 3.

**Table 3.** The proximate and ultimate analyses of the preheated char.

Item	Proximate Analysis (wt.%)					Ultimate Analysis (wt.%)			
	M <sub>ar</sub>	A <sub>ar</sub>	V <sub>ar</sub>	FC <sub>ar</sub>	C <sub>ar</sub>	H <sub>ar</sub>	O <sub>ar</sub>	N <sub>ar</sub>	S <sub>ar</sub>
@850 °C	1.20	14.54	5.15	79.11	80.80	1.21	0.68	0.99	0.59
@880 °C	1.21	14.39	4.81	79.59	81.63	1.16	/	1.01	0.60
@910 °C	0.59	14.61	4.41	80.40	82.05	1.17	/	0.93	0.65
@950 °C	0.75	16.42	3.53	79.31	80.20	1.00	/	0.99	0.64

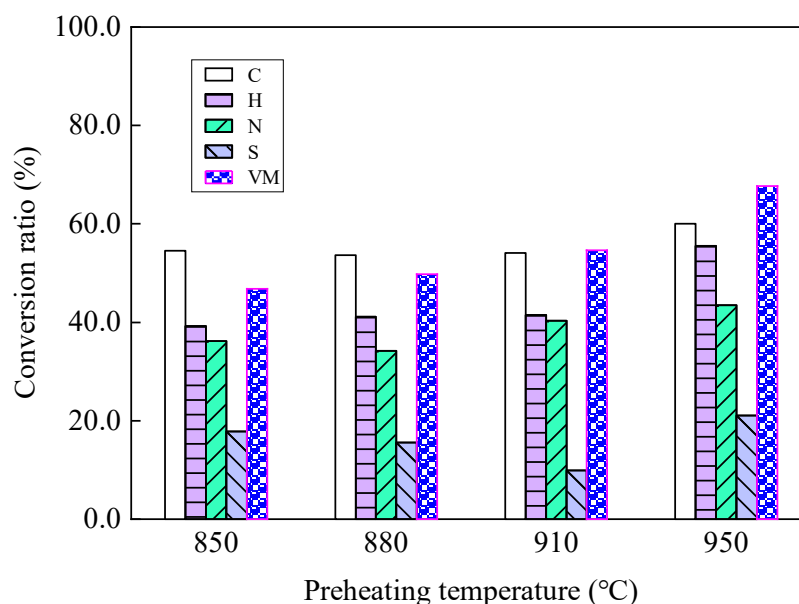
Note: “@” represents the preheated char samples at specific temperatures.

Using the ash balance method with the basic hypothesis that the ash content would remained unchanged [20,21], the ratio of conversion from semi-coke to preheated fuel for each component could be calculated as follows:

$$C_X = 1 - \frac{A_1 \times X_2}{A_2 \times X_1}, \quad (5)$$

where  $A_1$  is the ash content in the semi-coke,  $A_2$  is the ash content in the preheated char,  $X_1$  is the component X content in the semi-coke, and  $X_2$  is the component X content in the preheated char.

Figure 10 shows the conversion ratios for different species with different preheating temperatures, and almost over 50% of carbon was converted into coal gas, such as CO<sub>2</sub> or CO. The order of the conversion ratios was C > H > N > S. The conversion of S was the lowest because some of the inorganic sulfur did not undergo a conversion reaction [22,23]. Interestingly, at the condition with 910 °C, the conversion of S was lower than that with other temperatures, perhaps due to reactions of S with Ca occurring in the CFB. The ratio of carbon conversion was completely linear in relation to that of nitrogen. In contrast to findings for pulverized coal, the conversion of H was not the highest due to the lower H content in the semi-coke.

**Figure 10.** The conversion ratios for C/H/N/S/VM with different preheating temperatures.

When increasing the preheating temperature from 850 °C to 910 °C, the conversion ratio for carbon increased from 54.5% to 60.0% due to the gasification reaction of C and CO<sub>2</sub>. In addition, increasing the preheating temperature promoted the release of N fuel. Due to the strong reducing atmosphere in the CFB, most of the released N fuel was converted into

N<sub>2</sub>, providing an extremely important condition for realizing ultra-low NO<sub>x</sub> emissions for this system.

Comparing Tables 1 and 3, we found that, compared to the semi-coke, the volatile matter content increased for preheated char at 850 °C, 880 °C, and 910 °C due to the comprehensive effect of the multi-species content. However, what we want to emphasize is that, with the increase in the preheating temperature from 850 °C to 950 °C, the conversion ratio for volatile matter indeed increased continuously, as shown in Figure 10, meaning that more volatile matter was converted into coal gas.

### 3.4. Kinetic Analysis of the Semi-Coke and Preheated Char

The thermal gravity–differential thermal gravity (TG-DTG) curves for the samples are shown in Figure 11. We found that the maximum weight loss temperature occurred earlier for the preheated char than the raw semi-coke.

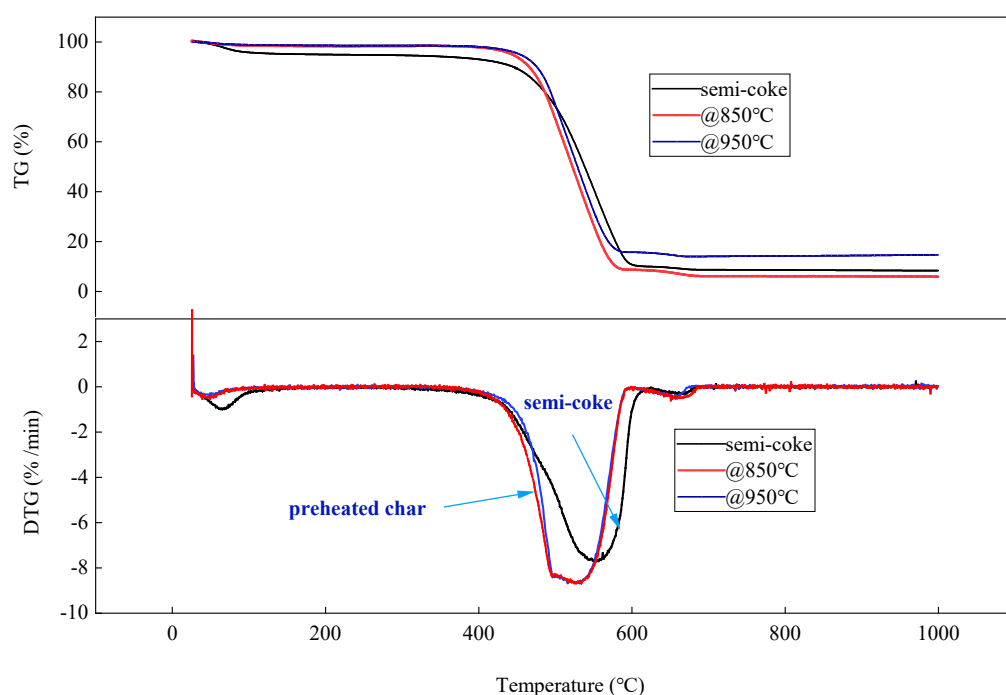


**Figure 11.** TG-DTG curves for the preheated char and semi-coke.

As shown in Figure 11, the ignition, burnout, and maximum weight loss temperatures were calculated and are listed in Table 4. The ignition and burnout temperatures for the preheated char decreased compared to those for the semi-coke, illustrating that the preheated char had better combustion characteristics. The reason was that during the process of fuel preheating in the CFB, some gases were released from the inside of the particles, which also made the structure of the inner pores develop with a large specific surface area. Zhang et al. [24] preheated anthracite with a specific surface area of 3.53 m<sup>2</sup>/g in a CFB and found that the specific surface area of the preheated char was enlarged to 67.1 m<sup>2</sup>/g, increasing by 19 times. The developed inner pores could facilitate the progress of the reactions, such as combustion or gasification.

**Table 4.** The ignition, burnout, and maximum weight loss temperatures.

Sample	Ignition Temperature (°C)	Burnout Temperature (°C)	Maximum Weight Loss Temperature (°C)
Semi-coke	472	581	551
@850 °C	464	565	533
@950 °C	465	563	526

The Coats–Redfern method was used to calculate the kinetic parameters with the following formula and the hypothesis of a first-order reaction [25,26]:

$$\ln \left[ \frac{-\ln(1-x)}{T^2} \right] = \ln \frac{AR}{\beta E} - \frac{E}{RT} \quad (6)$$

where  $x$  is the mass conversion ratio,  $T$  is the heating temperature (K),  $A$  represents the pre-exponential factor ( $\text{min}^{-1}$ ),  $E$  is the activation energy (kJ/mol),  $\beta$  is the heating rate ( $^{\circ}\text{C}/\text{min}$ ), and  $R$  is the gas constant ( $8.314 \times 10^{-3}$  kJ/(mol·K)).

The  $\ln(-\ln(1-x)/T^2)$  relationships for  $1/T$  with the raw semi-coke and preheated char are shown in Figure 12, with the linear fitting curve given by Origin software 2021. The slope of the curve was  $-E/R$ , and the intercept was  $\ln \frac{AR}{\beta E}$ . Thus, the activation energy  $E$  and pre-exponential factor  $A$  could be determined.

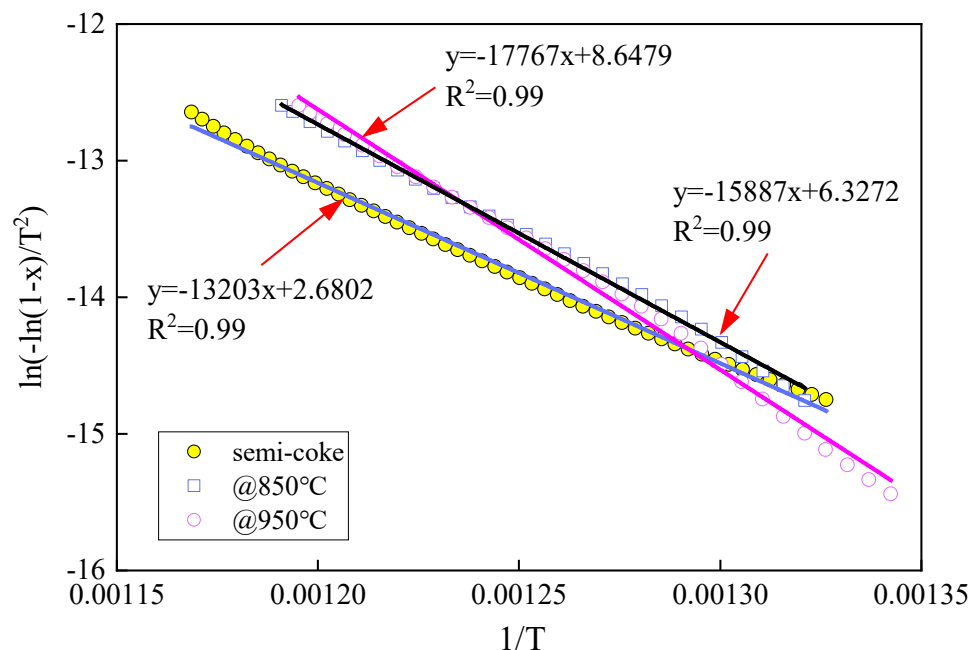
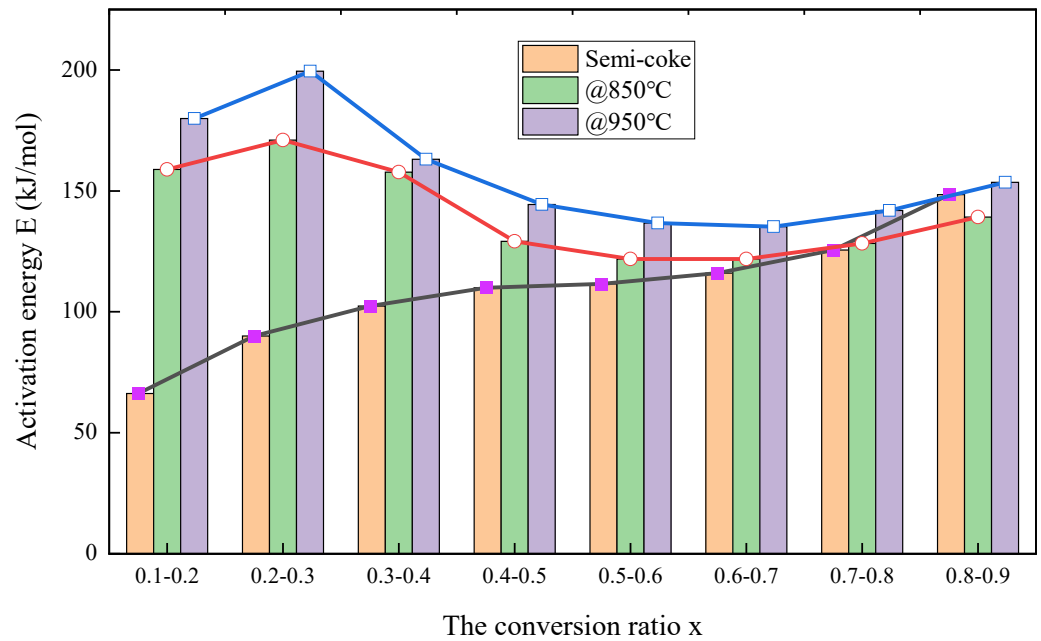


Figure 12. The  $\ln(-\ln(1-x))$  relationship for  $1/T$ .

The kinetic parameters with the different conversion ratios were calculated, as shown in Table 5. Figure 13 shows the activation energy distribution characteristics for the semi-coke and preheated char with different conversion ratios.

Table 5. The kinetic parameters with different conversion ratios.

Conversion Ratio	Semi-Coke			@850 °C			@950 °C		
	$E$ (kJ/mol)	$A$ ( $\text{min}^{-1}$ )	$R^2$	$E$ (kJ·mol)	$A$ ( $\text{min}^{-1}$ )	$R^2$	$E$ (kJ/mol)	$A$ ( $\text{min}^{-1}$ )	$R^2$
0.1–0.2	66.3	1196	0.99	158.9	$6.8 \times 10^9$	0.99	179.9	$1.7 \times 10^{11}$	0.99
0.2–0.3	90.0	$7.3 \times 10^4$	0.99	171.0	$5.0 \times 10^{10}$	0.99	199.5	$4.2 \times 10^{12}$	0.99
0.3–0.4	102.4	$5.6 \times 10^5$	0.99	157.7	$5.7 \times 10^9$	0.99	163.1	$1.2 \times 10^{10}$	0.99
0.4–0.5	110.0	$1.9 \times 10^6$	1.00	129.2	$5.7 \times 10^7$	0.99	144.4	$6.1 \times 10^8$	0.99
0.5–0.6	111.6	$2.4 \times 10^6$	0.99	121.9	$1.8 \times 10^7$	1.00	136.7	$1.7 \times 10^8$	1.00
0.6–0.7	116.0	$4.9 \times 10^6$	0.99	121.8	$1.7 \times 10^7$	1.00	135.2	$1.4 \times 10^8$	1.00
0.7–0.8	125.6	$2.1 \times 10^7$	0.99	128.3	$4.9 \times 10^7$	0.99	141.9	$4.0 \times 10^8$	0.99
0.8–0.9	148.5	$6.6 \times 10^8$	0.99	139.2	$2.6 \times 10^8$	0.99	153.6	$2.4 \times 10^9$	0.99
Average	109.8	$1.9 \times 10^6$	0.99	132.1	$8.8 \times 10^7$	0.99	147.7	$1.0 \times 10^9$	0.99



**Figure 13.** The activation energy distribution with staged conversion ratios.

Interestingly, compared to the semi-coke, although the activation energy  $E$  of the preheated char increased, the pre-exponential factor  $A$  also significantly increased. For the semi-coke, the activation energy increased with an increasing conversion ratio, while for the preheated char, the activation energy showed a decreasing tendency with an increasing conversion ratio.

To further explain the effect of preheating on the fuel reaction characteristics, the reaction rate constant  $k$  was obtained using the Arrhenius formula, as expressed by [27]:

$$k = A \exp\left(-\frac{E}{RT}\right). \quad (7)$$

The reaction rate constant  $k$  values for the raw semi-coke and preheated char with different temperatures are shown in Figure 14.

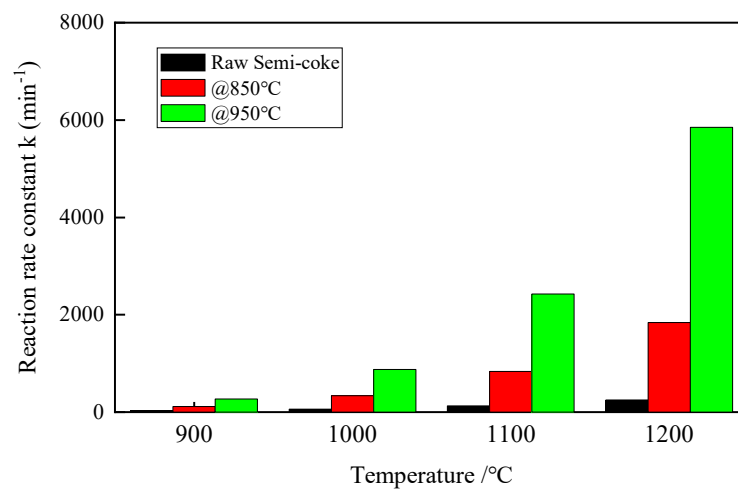


**Figure 14.** The comparison of  $k$  for the raw semi-coke and preheated char.

The reaction rate constant for the preheated char at 950 °C was 20 times higher than that for the semi-coke when the combustion temperature was higher than 1100 °C, which provided a very important condition for the high-efficiency combustion of the preheated fuel.

Three models [28]—namely, the homogenous reaction model (HRM), the shrinking core model (SCM), and the modified volumetric reaction model (MVRM)—were used to describe the variations in the conversion ratio with time.

The HRM was defined as a first-order reaction with the hypothesis that the particle size would not change in the reaction process, and the conversion ratio could be expressed by:

$$\frac{dx}{dt} = k(1 - x), \quad (8)$$

and its integral transformation expression equation:

$$-\ln(1 - x) = kt, \quad (9)$$

where  $t$  is time and  $k$  is a constant. In this model, the  $k$  value was first determined by fitting the experimental data, and then  $x$  could be calculated based on this HRM.

In the SCM, the hypothesis was that the particle size would vary with time. The reaction rate could be described by:

$$\frac{dx}{dt} = k(1 - x)^{2/3}. \quad (10)$$

For this expression, the equation was integrated and changed into a new exponential expression as follows:

$$3 \left[ 1 - (1 - x)^{1/3} \right] = kt. \quad (11)$$

The MVRM improved the homogeneous volumetric reaction model and proved to be more suitable with variable reaction rates. In the MVRM, the solution function could be the same with Formula (8), where  $k$  could be described by:

$$k = A_i^{1/B_i} B_i \left[ -\ln(1 - x)^{\frac{B_i-1}{B_i}} \right], \quad (12)$$

and  $x$  could be expressed by:

$$x = 1 - \exp(-A_i t^{B_i}). \quad (13)$$

In this calculation, the  $i$  value was 4, indicating that the calculation was divided into four stages for accurate prediction.

A comparison of the experimental and simulation data with the different models is shown in Figure 15. We observed that the MVRM model showed good agreement with the experimental data, and the worst predictions for the semi-coke or preheated char were given by the HRM model.

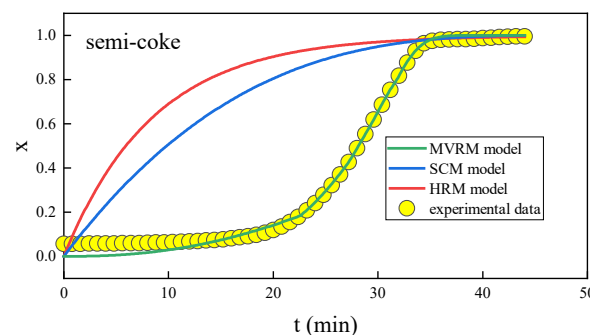
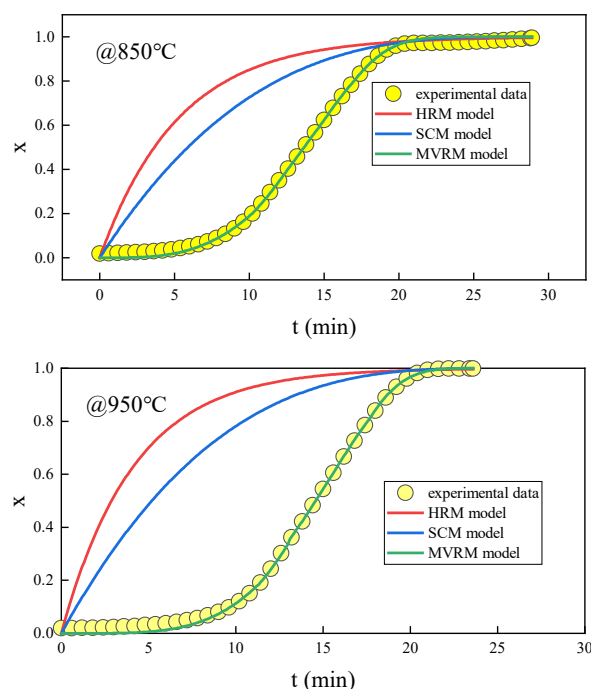


Figure 15. Cont.



**Figure 15.** Comparison of the simulation data and the experimental data.

#### 4. Conclusions

Due to its low volatile content, semi-coke has difficulties with ignition and burnout. Preheating in a CFB before combustion was found to be a good solution to this problem. Several experiments were performed. The main conclusions are as follows:

- (1) There was a strong reducing atmosphere in the CFB with an air equivalence ratio of 0.3, and the temperature was quite stable with a temperature difference lower than 50 °C, indicating a uniform preheating process;
- (2) As the preheating temperature increased, the ratio of CO/CO<sub>2</sub> significantly increased, which was due to the gasification reaction of CO<sub>2</sub> and C intensifying at temperatures higher than 900 °C. The maximum heating value for the coal gas was 3.7 MJ/m<sup>3</sup> and the production rate was 2.57 m<sup>3</sup>/kg when the preheating temperature was 950 °C;
- (3) Using the ash balance method, the conversion ratios for different species were calculated. Over 50% of carbon was converted into CO or CO<sub>2</sub>, and the conversion of the different species followed the order C > H > N > S. The conversion ratio for carbon was linear in relation to that of nitrogen, and the conversion ratio for sulfur was the lowest due to the presence of inorganic sulfur in the ash;
- (4) Thermogravimetric analysis was used to evaluate the kinetic characteristics of the semi-coke and preheated char. The results showed that the ignition and burnout temperatures of the preheated char were lower than those of the semi-coke. The activation energy of the preheated char increased but with a larger pre-exponential factor. The reaction rate constant for the preheated char was 20 times higher than that for the semi-coke when the temperature reached 1100 °C, which supplied a basis for the high-efficiency combustion of the preheated char in the following combustor;
- (5) Three models—namely, the HRM, SCM, and MVRM—were used to describe the variations in the conversion ratios with time for the semi-coke and preheated char. The results indicated that the modified volumetric reaction model agreed well with the experiment.

**Supplementary Materials:** The following supporting information can be downloaded at: <https://www.mdpi.com/article/10.3390/en16104124/s1>.

**Author Contributions:** Conceptualization and experimental scheme, J.Z. (Jianguo Zhu); experiments and sample analyses, J.Z. (Jiahang Zhang); kinetic model, J.L. All authors have read and agreed to the published version of the manuscript.

**Funding:** This research was funded by the Strategic Priority Research Program of the Chinese Academy of Sciences, grant number XDA29010100.

**Data Availability Statement:** The data presented in this study are available in the Supplementary Materials.

**Acknowledgments:** This work was supported by the project of the Strategic Priority Research Program of the Chinese Academy of Sciences. We also sincerely thank the Laboratory of Circulating Fluidized Bed, Institute of Engineering Thermophysics, Chinese Academy of Sciences, for providing the experiment platform and experimental conditions.

**Conflicts of Interest:** The authors declare no conflict of interest.

## References

1. Yao, H.F.; He, B.S.; Ding, G.C.; Tong, W.X.; Kuang, Y.C. Thermogravimetric analyses of oxy-fuel co-combustion of semi-coke and bituminous coal. *Appl. Therm. Eng.* **2019**, *156*, 708–721. [\[CrossRef\]](#)
2. Scaccia, S. Analysis and distribution of volatile gases from catalytic pyrolysis of Sulcis low-rank coal. *J. Anal. Appl. Pyrolysis* **2023**, *169*, 105820. [\[CrossRef\]](#)
3. Liu, J.J.; Wang, M.Y.; Liu, S.J.; Shangguan, J.; Yang, S. Cohesive components in coal and their cohesive mechanism during pyrolysis. *J. Anal. Appl. Pyrolysis* **2023**, *170*, 105871. [\[CrossRef\]](#)
4. Wang, C.W.; Wang, C.A.; Tang, G.T.; Zhang, J.M.; Gao, X.Y.; Che, D.F. Co-combustion behaviors and NO formation characteristics of semi-coke and antibiotic filter residue under oxy-fuel condition. *Fuel* **2022**, *319*, 123779. [\[CrossRef\]](#)
5. Wang, P.Q.; Wang, C.A.; Yuan, M.B.; Wang, C.W.; Zhang, J.P.; Du, Y.B.; Tao, Z.C.; Che, D.F. Experimental evaluation on co-combustion characteristics of semi-coke and coal under enhanced high-temperature and strong-reducing atmosphere. *Appl. Energy* **2020**, *260*, 114203. [\[CrossRef\]](#)
6. Li, Z.Y.; Niu, S.L.; Han, K.H.; Li, Y.J.; Wang, Y.Z.; Lu, C.M. Thermogravimetric analysis on the characteristics of oxy-fuel co-combustion of sub-bituminous coal and semi-coke. *J. Fuel Chem. Technol.* **2022**, *50*, 937–951. [\[CrossRef\]](#)
7. Zheng, S.W.; Hu, Y.J.; Wang, Z.Q.; Cheng, X.X. Experimental investigation on ignition and burnout characteristics of semi-coke and bituminous coal blends. *J. Energy Inst.* **2020**, *93*, 1373–1381. [\[CrossRef\]](#)
8. Du, Y.B.; Wang, C.A.; Wang, P.Q.; Meng, Y.; Wang, Z.C.; Yao, W.; Che, D.F. Computational fluid dynamics investigation on the effect of co-firing semi-coke and bituminous coal in a 300 MW tangentially fired boiler. *Proc. Inst. Mech. Eng. Part A J. Power Energy* **2019**, *233*, 221–231. [\[CrossRef\]](#)
9. Wang, P.Q.; Wang, C.A.; Wang, C.W.; Yuan, M.B.; Du, Y.B.; Zhang, J.P.; Che, D.F. Synergistic effects in rapid co-pyrolysis of semi-coke and coal at high temperature. *Fuel* **2020**, *282*, 118795. [\[CrossRef\]](#)
10. Zhang, Y.; Zhu, J.G.; Lyu, Q.G.; Pan, F.; Zhu, S.J. Characteristics of preheating combustion of power coal with high coking properties. *J. Therm. Sci.* **2021**, *30*, 1108–1115. [\[CrossRef\]](#)
11. Zhu, S.J.; Lyu, Q.G.; Zhu, J.G. Experimental investigation of NO<sub>x</sub> emissions during pulverized char combustion in oxygen-enriched air preheated with a circulating fluidized bed. *J. Energy Inst.* **2019**, *92*, 1388–1398. [\[CrossRef\]](#)
12. Suda, T.; Takafuji, M.; Hirata, T.; Yoshino, M.; Sato, J. A study of combustion behavior of pulverized coal in high-temperature air. *Proc. Combust. Inst.* **2002**, *29*, 503–509. [\[CrossRef\]](#)
13. Lv, Z.M.; Xiong, X.H.; Ruan, R.H.; Wang, Y.B.; Tan, H.Z. NO emission and burnout characteristics in co-combustion of coal and sewage sludge following high-temperature preheating. *Fuel* **2023**, *331*, 125887. [\[CrossRef\]](#)
14. Lv, Z.M.; Xiong, X.H.; Tan, H.Z.; Wang, X.B.; Liu, X.; ur Rahman, Z. Experimental investigation on NO emission and burnout characteristics of high-temperature char under the improved preheating combustion technology. *Fuel* **2022**, *313*, 122662. [\[CrossRef\]](#)
15. Liu, J.Z.; Liu, Y.H.; Zhu, J.G.; Ouyang, Z.Q.; Man, C.B.; Zhu, S.J.; Zhang, Y.; Lyu, Q.G. Bituminous coal deep regulated ultra-low NO flameless combustion with fluidized self-preheating fuel: A 2 MWth experimental study. *Fuel* **2021**, *294*, 120549. [\[CrossRef\]](#)
16. Ouyang, Z.Q.; Ding, H.L.; Liu, W.; Li, S.Y.; Cao, X.Y. Effect of the staged secondary air on NO emission of pulverized semi-coke flameless combustion with coal preheating technology. *Fuel* **2021**, *291*, 120137. [\[CrossRef\]](#)
17. Liu, W.; Ouyang, Z.Q.; Na, Y.J.; Cao, X.Y.; Liu, D.F.; Zhu, S.J. Effects of the tertiary air injection port on semi-coke flameless combustion with coal self-preheating technology. *Fuel* **2020**, *271*, 117640. [\[CrossRef\]](#)
18. GB/T 28731-2012; Proximate analysis of solid biofuels. Standards Press of China: Beijing, China, 2013.
19. Liang, C.; Wang, X.F.; Lyu, Q.G. Experimental investigation on fluidized modification in gasification of preheated coal using oxygen and steam. *Fuel* **2021**, *304*, 121375. [\[CrossRef\]](#)
20. Zhang, Z.; Chen, D.G.; Li, Z.S.; Cai, N.S.; Imada, J. Development of sulfur release and reaction model for computational fluid dynamics modeling in sub-bituminous coal combustion. *Energy Fuels* **2017**, *31*, 1383–1398. [\[CrossRef\]](#)
21. Ouyang, Z.Q.; Liu, W.; Man, C.B.; Zhu, J.G.; Liu, J.Z. Experimental study on combustion, flame and NO<sub>x</sub> emission of pulverized coal preheated by a preheating burner. *Fuel Process. Technol.* **2018**, *179*, 197–202. [\[CrossRef\]](#)

22. Schofield, K. The kinetic nature of sulfur's chemistry in flames. *Combust. Flame* **2001**, *124*, 137–155. [[CrossRef](#)]
23. Ströhle, J.; Chen, X.; Zorbach, I.; Epple, B. Validation of a detailed reaction mechanism for sulfur species in coal combustion. *Combust. Sci. Technol.* **2014**, *186*, 540–551. [[CrossRef](#)]
24. Zhang, X.Y.; Zhu, S.J.; Zhu, J.G.; Liu, Y.H.; Zhang, J.H.; Hui, J.C.; Ding, H.L.; Cao, X.Y.; Lyu, Q.G. Preheating and combustion characteristics of anthracite under O<sub>2</sub>/N<sub>2</sub>, O<sub>2</sub>/CO<sub>2</sub> and O<sub>2</sub>/CO<sub>2</sub>/H<sub>2</sub>O atmosphere. *Energy* **2023**, *274*, 127419. [[CrossRef](#)]
25. Ma, M.; Bai, Y.H.; Song, X.D.; Wang, J.F.; Su, W.G.; Yao, M.; Yu, G.S. Investigation into the co-pyrolysis behaviors of cow manure and coal blending by TG–MS. *Sci. Total Environ.* **2020**, *728*, 138828. [[CrossRef](#)] [[PubMed](#)]
26. Bai, H.C.; Mao, N.; Wang, R.H.; Li, Z.M.; Zhu, M.L.; Wang, Q. Kinetic characteristics and reactive behaviors of HSW vitrinite coal pyrolysis: A comprehensive analysis based on TG-MS experiments, kinetics models and ReaxFF MD simulations. *Energy Rep.* **2021**, *7*, 1416–1435. [[CrossRef](#)]
27. Li, J.Z.; Li, M.N.; Zhang, Y.M.; Zhang, W.; Qiao, P. Research on the pyrolysis characteristics and kinetics of two typical inferior heavy oils. *Fuel* **2022**, *328*, 125330. [[CrossRef](#)]
28. Liu, J.Z.; Liu, Y.H.; Zhu, J.G.; Lyu, Q.G.; Pan, F.; Zhang, Y.; Zhang, J.H. A novel developed weighted exponential sum model for char cloud conversion behavior under air- and oxy-combustion: Experiments and kinetics modeling analysis. *Combust. Flame* **2021**, *231*, 111489. [[CrossRef](#)]

**Disclaimer/Publisher's Note:** The statements, opinions and data contained in all publications are solely those of the individual author(s) and contributor(s) and not of MDPI and/or the editor(s). MDPI and/or the editor(s) disclaim responsibility for any injury to people or property resulting from any ideas, methods, instructions or products referred to in the content.